A parametric investigation of natural ventilation flow with a line heat source

T. Hattori[1] S. W. Armfield[2] M. P. Kirkpatrick[3]

(Received 27 January 2011; revised 1 December 2011)

Abstract

The effects of Reynolds number (Re) and Prandtl number (Pr) on fully-developed, transitional natural ventilation flow with a line heat source are investigated using two dimensional direct numerical simulations. The flow is simulated in the range, $5.0 \times 10^5 \leqslant \mathrm{Re} \leqslant 1.58 \times 10^6$ and $0.7 \leqslant \mathrm{Pr} \leqslant 70$. The initial development of the flow is also investigated and scaling relationships are obtained for initial peak velocity, time taken to reach the initial peak and time taken for the onset of instability. Spectral amplitudes are shown to reduce with increasing Pr. In lower Pr flows, large amplitude motions occur at higher frequencies than for higher Pr. The interface height is found to vary with the parameter values, and the upper layer temperature distribution is found to be more uniform at lower Pr.

http://journal.austms.org.au/ojs/index.php/ANZIAMJ/article/view/3925 gives this article, © Austral. Mathematical Soc. 2012. Published January 5, 2012. ISSN 1446-8735. (Print two pages per sheet of paper.)

Contents

1 Introduction **C1061**

2 Numerical method **C1062**

3 Results and discussion **C1065**
3.1 Initial flow development C1065
3.2 Flow turbulence C1073
3.3 Mean temperature field C1075

4 Conclusion **C1079**

References **C1080**

1 Introduction

Displacement cooling flow has been extensively studied, both analytically and experimentally, by Linden et al. [11]. This flow may be thought of as a semi-confined plume flow, which involves complex interaction of a thermal plume with the upper stratified fluid layer and the associated mixing. Linden et al. [11] developed a mathematical model for the steady state height of the interface that forms between lower ambient and upper buoyant fluids for the case of a fully turbulent plume, assuming the plume theory of Morton et al. [13]. For a fully turbulent plume, the turbulent Prandtl number (Pr) is dominant and the plume is almost independent of the physical properties of the fluid [6]. Hence, the analytical solutions developed by Morton et al. [13] exclude the effect of the molecular Prandtl number (Pr). Linden et al. [11] further assumed a sharp interface formed between the upper buoyant and lower ambient layers and the uniformity of the upper layer buoyancy, and found that the interface height is independent of Reynolds number (Re) and Pr.

The current study extends the work of Linden et al. [11] on the flow in a fully turbulent regime to that in a transitional regime to investigate the effects of Re on the flow initiation and of both Re and Pr on the fully developed characteristics, including the flow turbulence and the mean temperature distribution. Our approach in the study of the flow initiation is similar to that of Bastiaans et al. [4], an investigation of a fully confined planar plume in the transitional regime, although in that case results were obtained for constant Re and Pr with varying amplitudes of an external disturbance to examine the effect of the disturbance on the loss of stability.

2 Numerical method

We employ two dimensional direct numerical simulation to solve the non-dimensional, incompressible Navier–Stokes equations, with the Boussinesq assumption for buoyancy, for transitional natural ventilation flow with a line heat flux source. The governing equations are

$$\frac{\partial u_i}{\partial t} + \frac{\partial (u_j u_i)}{\partial x_j} = \frac{1}{\mathrm{Re}} \frac{\partial}{\partial x_j} \left(\frac{\partial u_i}{\partial x_j} \right) - \frac{dp}{dx_i} + T\delta_{i2}\,, \tag{1}$$

$$\frac{\partial T}{\partial t} + \frac{\partial (u_j T)}{\partial x_j} = \frac{1}{\mathrm{Re}\,\mathrm{Pr}} \frac{\partial}{\partial x_j} \left(\frac{\partial T}{\partial x_j} \right), \tag{2}$$

$$\frac{\partial u_i}{\partial x_i} = 0\,, \tag{3}$$

where $i = 1, 2$ and $j = 1, 2$, $x_1 = x$ and $x_2 = y$ are the coordinates as shown in Figure 1, and t is time. The velocity components, $u_1 = u$ and $u_2 = v$, are in the x and y directions, respectively, p is the pressure perturbation, and T the temperature perturbation. The control parameters are:

$$\mathrm{Re} = \frac{UH}{\nu}\,, \tag{4}$$

$$\mathrm{Pr} = \frac{\nu}{\kappa}\,. \tag{5}$$

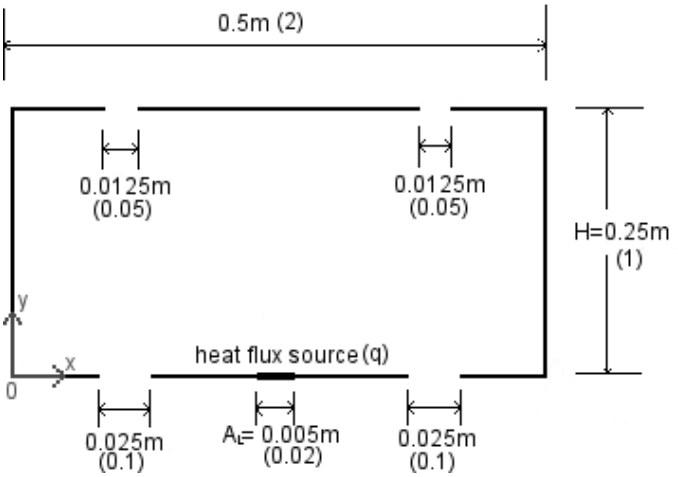

Figure 1: Geometry considered (the non-dimensional lengths are given in brackets).

The characteristic velocity, U, is defined as $U = \sqrt{g\beta H^2 q/(kA_L)}$, where g is the gravitational acceleration, β the thermal expansion coefficient, q the source heat flux per unit length, k the thermal conductivity, A_L the source area per unit length, H the domain height, ν is the kinematic viscosity, and κ the thermal diffusivity in the equations above. Numerical results are presented and discussed for fully developed flows at $Re = 5.0 \times 10^5$, 1.0×10^6 and 1.58×10^6 and $Pr = 0.7$, 7 and 70, and for start-up flows with $2.5 \times 10^5 \leqslant Re \leqslant 1.0 \times 10^6$ and $Pr = 7$. The computational domain is shown in Figure 1.

A non-staggered, Cartesian grid is used, and Equations (1)–(3) are solved using the finite volume method. A nonuniform mesh is used to provide the greatest resolution near the heat source and the openings. Fourth order central spatial differencing with the ULTRA (Universal Limiter for Tight Resolution and Accuracy) flux limiter [10] is employed for the advection term in Equation (2) to avoid instability due to a large local Peclet number for the cases with high Pr (= 7 and 70). Second order central spatial differencing

is employed otherwise. The Adams–Bashforth and the Crank–Nicolson time discretisation schemes are employed for the advection and diffusion terms, respectively. The fractional step method [3] with the velocity interpolation scheme of Armfield [2] is used for the velocity-pressure coupling. The code was written in the FORTRAN90 language. The boundary conditions are as follows.

- On closed boundaries, the no-slip condition is applied for velocity and the Neumann condition with zero derivative for the pressure correction. Pressure on the node outside the boundary is obtained by a second order extrapolation from interior nodes.
- On open boundaries, the tangential velocity and the pressure correction are set to zero. On the top openings, the Neumann condition with zero derivative is applied for the normal velocity component, and pressure is set to zero on the node outside the boundary. On the bottom openings, the normal velocity component is calculated such that the rate of inflow through the bottom openings is equal to the rate of outflow through the top openings, with pressure on the node outside the boundary obtained by a second order extrapolation from interior nodes.
- Boundaries are all adiabatic except for the source and the inlets. At the heat flux source, $\partial T/\partial y$ is set to -1, and the inflow temperature is set to $T = 0$.

For the determination of grids, it is important to consider the smallest length scales of the flow: the viscous scale, η_ν, and the thermal diffusion scale, η_κ. They are known to have the scaling relationships, $\eta_\nu \sim \mathrm{Re}^{-1/2}$ and $\eta_\kappa \sim (\mathrm{Re}\,\mathrm{Pr})^{-1/2}$ for two dimensional flows [5]. Thus, η_κ reduces with increasing Pr, hence a finer grid is required for simulations of higher Pr flows. Therefore, grid dependency is examined for the high Pr cases, $\mathrm{Pr} = 7$ and 70, with $\mathrm{Re} = 5.0 \times 10^5$ and 1.58×10^6, as shown in Figure 2. Here, mean temperature refers to temporal mean obtained over 3–4.5 million time steps, spatially averaged across the domain width. For $\mathrm{Pr} = 7$ and $\mathrm{Re} = 5.0 \times 10^5$, the 453×325 mesh, with smallest grid size of 0.0015, is considered sufficiently

Table 1: Summary of mesh resolutions and time steps (Δt).

Pr \ Re	5.0×10^5	1.0×10^6	1.58×10^6
0.7	453×325 $\Delta t = 3.0 \times 10^{-3}$	603×425 $\Delta t = 2.0 \times 10^{-3}$	603×425 $\Delta t = 1.5 \times 10^{-3}$
7	453×325 $\Delta t = 1.0 \times 10^{-2}$	603×425 $\Delta t = 7.5 \times 10^{-3}$	603×425 $\Delta t = 5.0 \times 10^{-3}$
70	603×425 $\Delta t = 1.5 \times 10^{-2}$	603×425 $\Delta t = 1.0 \times 10^{-2}$	603×425 $\Delta t = 1.0 \times 10^{-2}$

fine. For the cases of $\mathrm{Re} = 1.58 \times 10^6$ with both Pr, the 603×425 mesh, with smallest grid size of 0.001, is considered sufficiently fine. In the case of $\mathrm{Pr} = 70$ and $\mathrm{Re} = 5.0 \times 10^5$, the results for the two mesh resolutions show a larger deviation, so we use the 603×425 mesh. Time steps are determined so that the Courant number is typically in the range 0.015—0.03. The mesh resolutions and time steps used to obtain results for fully developed flows (Sections 3.2 and 3.3) are summarised in Table 1. For the investigation of start-up flows, the results are obtained using the 603×425 mesh and a time step of 7.5×10^{-3} for all the cases (Section 3.1).

3 Results and discussion

3.1 Initial flow development

For the investigation of start-up flows, the results are obtained for $2.5 \times 10^5 \leqslant \mathrm{Re} \leqslant 1.0 \times 10^6$ and a fixed $\mathrm{Pr} = 7$. In the given range of Re and Pr, the breakdown of the symmetric flow into oscillatory flow, which is associated with the onset of turbulence, occurs sometime after the plume reaches the ceiling.

Figures 3–8 show contours of instantaneous temperature fields at different

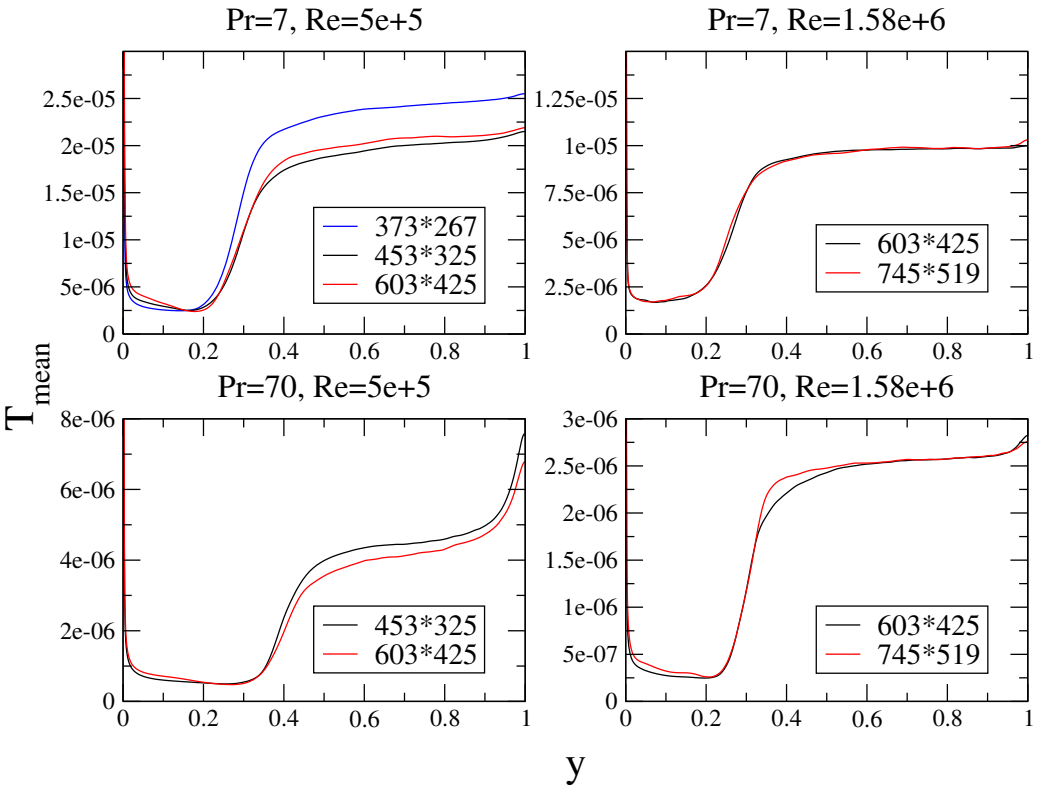

Figure 2: Mean temperature over height for $\mathrm{Re} = 5.0 \times 10^5$ and 1.58×10^6 and $\mathrm{Pr} = 7$ and 70 with different mesh resolutions

times for $\mathrm{Re} = 1.0 \times 10^6$. Vorticity fields are also shown for $t = 675.0$ and 806.25. At early times (Figures 3a and 3b), the start-up plume grows towards the ceiling, maintaining the symmetric dipolar structure. A similar structure was observed by Bastiaans et al. [4]. The dipolar structure collides with the ceiling at $t \approx 560$. Then it splits into two monopole vortex structures (Figures 4a and 5a). Flow symmetry is still maintained at this stage. Figure 5a shows a pair of strong vortex sheets at the ceiling, with opposite signs to those of the primary vortices. The creation of these secondary vortices

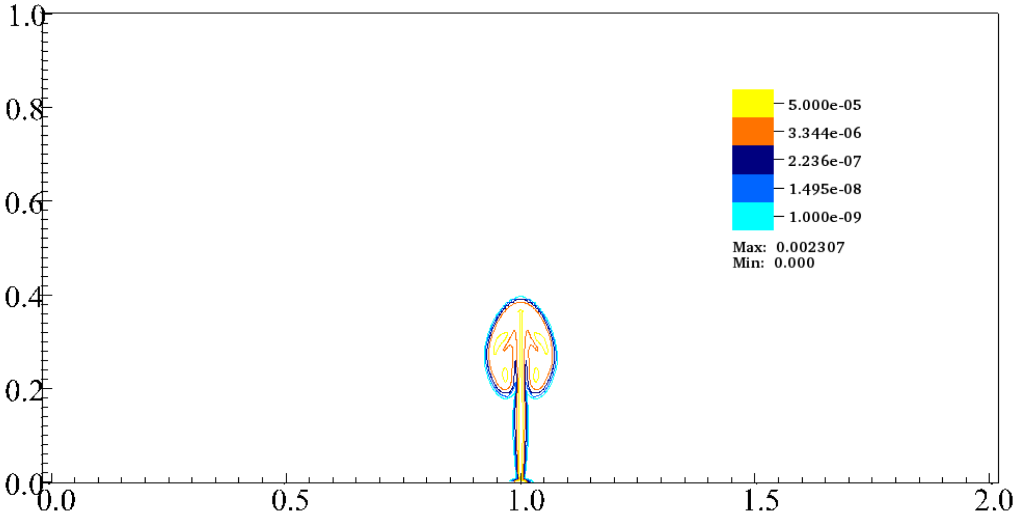

(a) t = 262.5

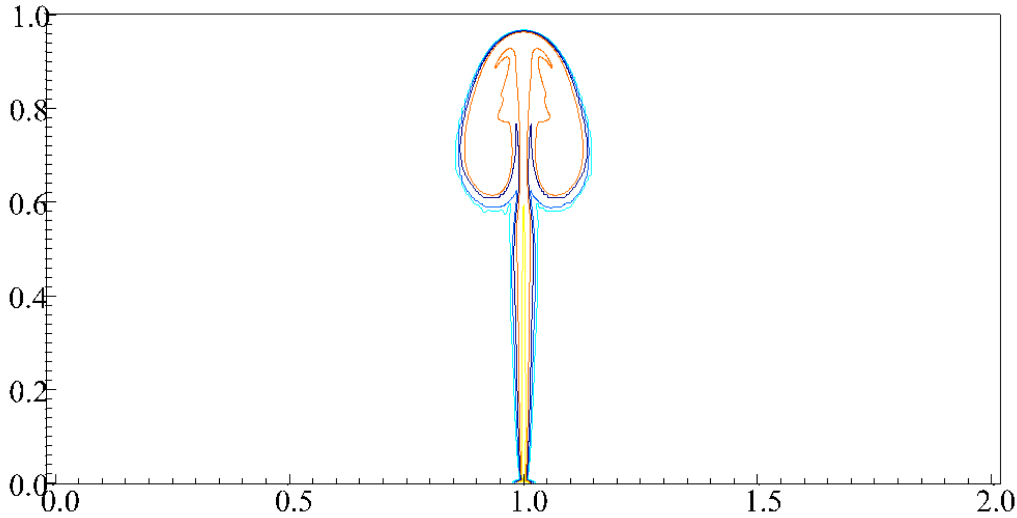

(b) t = 525.0

Figure 3: Flow development over time for Pr = 7 and Re = 1.0×10^6. Figures 3a–4b and 6a–8b show temperature contours, whereas Figures 5a–5b show vorticity fields.

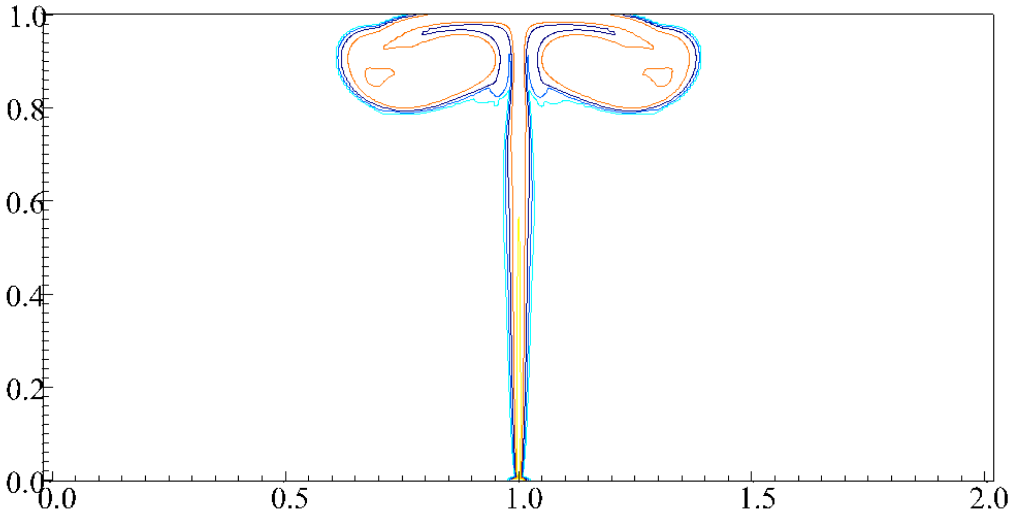

(a) t = 675.0

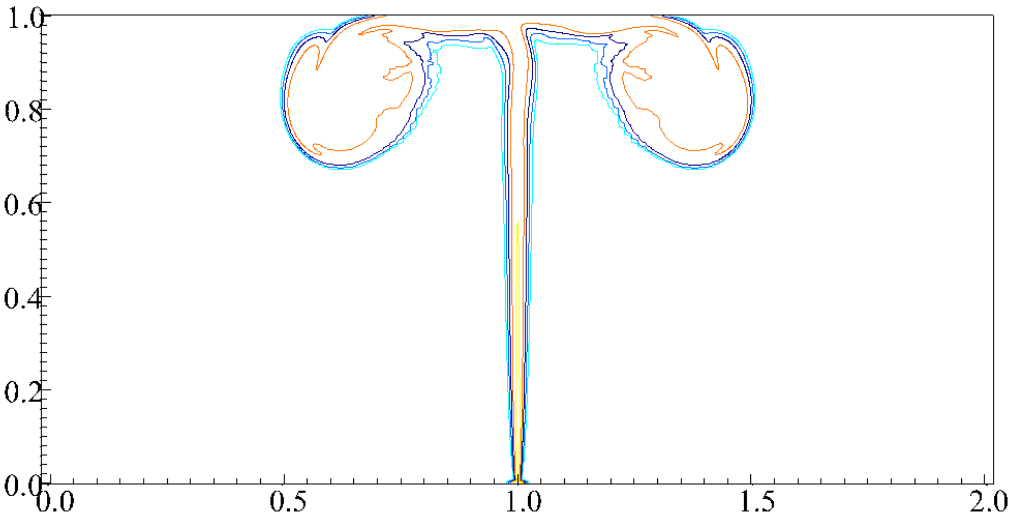

(b) t = 806.25

Figure 4: Flow development over time for Pr = 7 and Re = 1.0×10^6. Figures 3a–4b and 6a–8b show temperature contours, whereas Figures 5a–5b show vorticity fields.

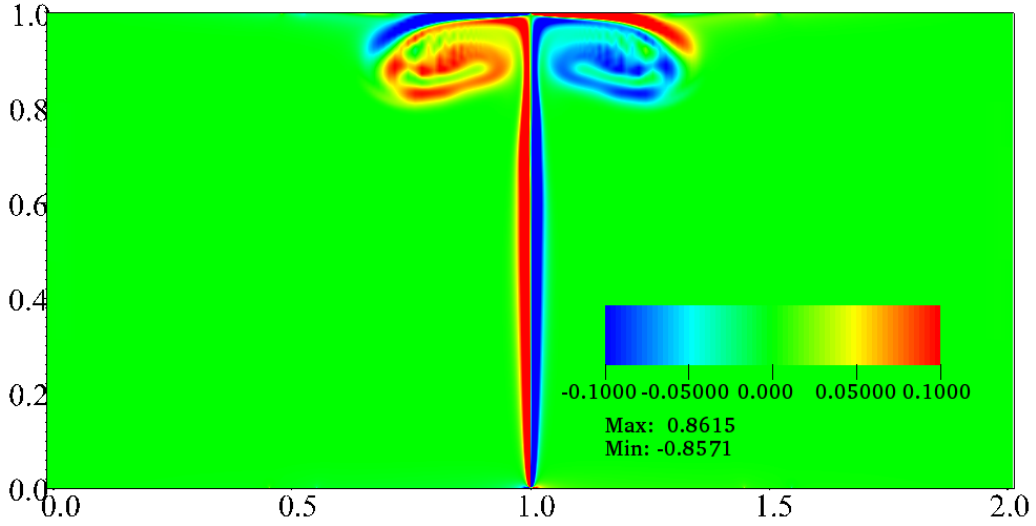

(a) t = 675.0

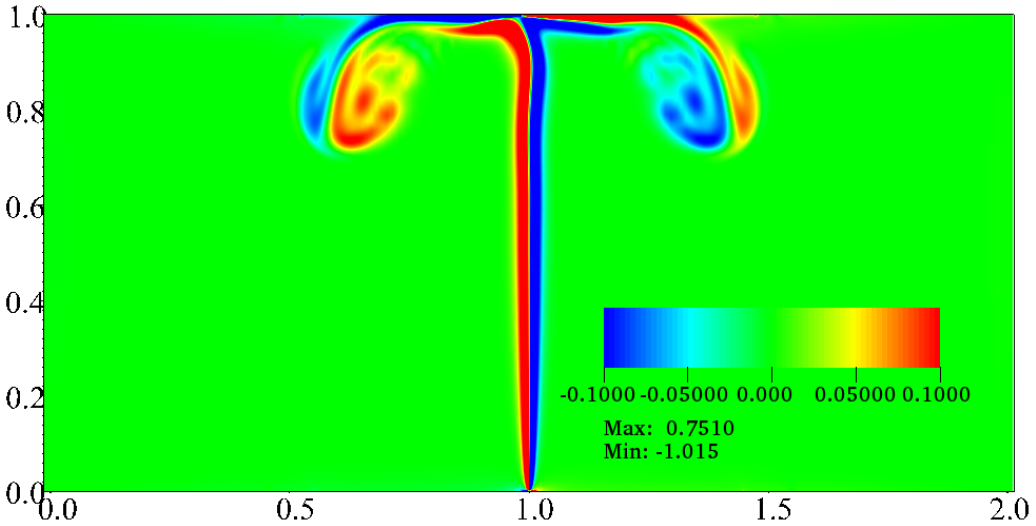

(b) t = 806.25

Figure 5: Flow development over time for Pr = 7 and Re = 1.0×10^6. Figures 3a–4b and 6a–8b show temperature contours, whereas Figures 5a–5b show vorticity fields.

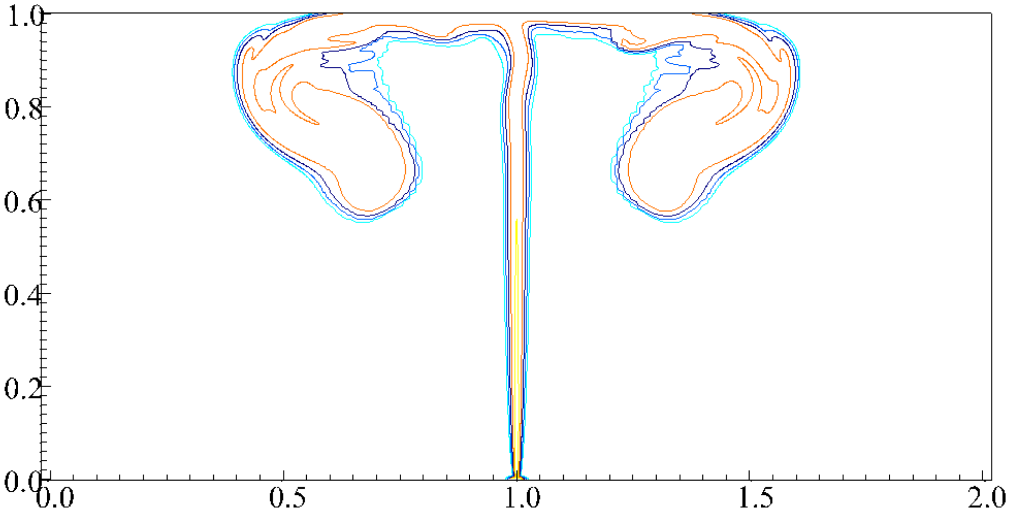

(a) t = 956.25

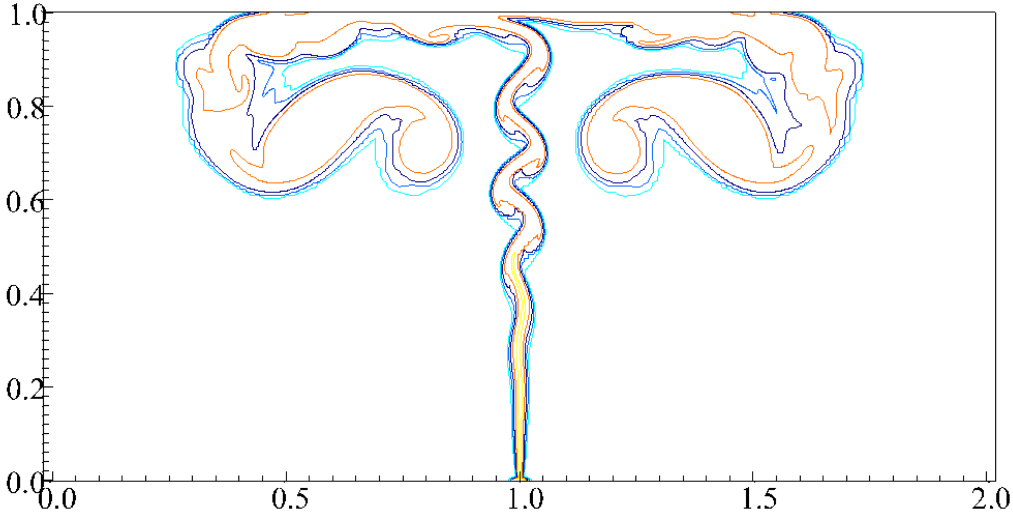

(b) t = 1106.25

Figure 6: Flow development over time for Pr = 7 and Re = 1.0×10^6. Figures 3a–4b and 6a–8b show temperature contours, whereas Figures 5a–5b show vorticity fields.

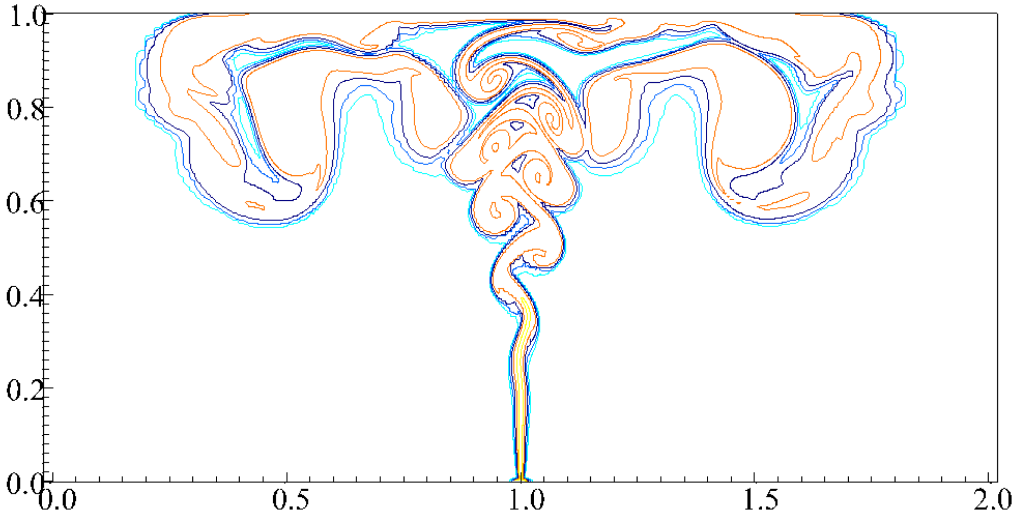

(a) t = 1218.75

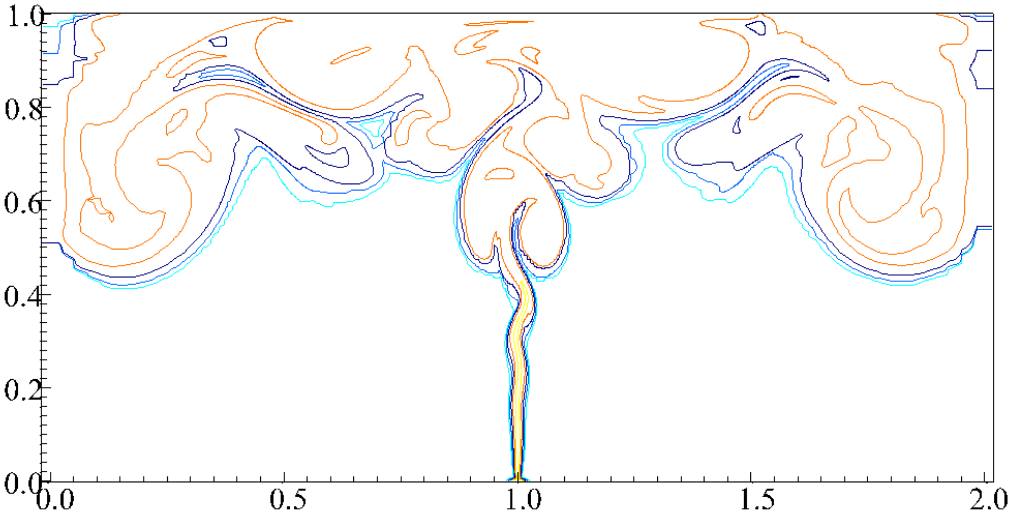

(b) t = 1631.25

Figure 7: Flow development over time for Pr = 7 and Re = 1.0×10^6. Figures 3a–4b and 6a–8b show temperature contours, whereas Figures 5a–5b show vorticity fields.

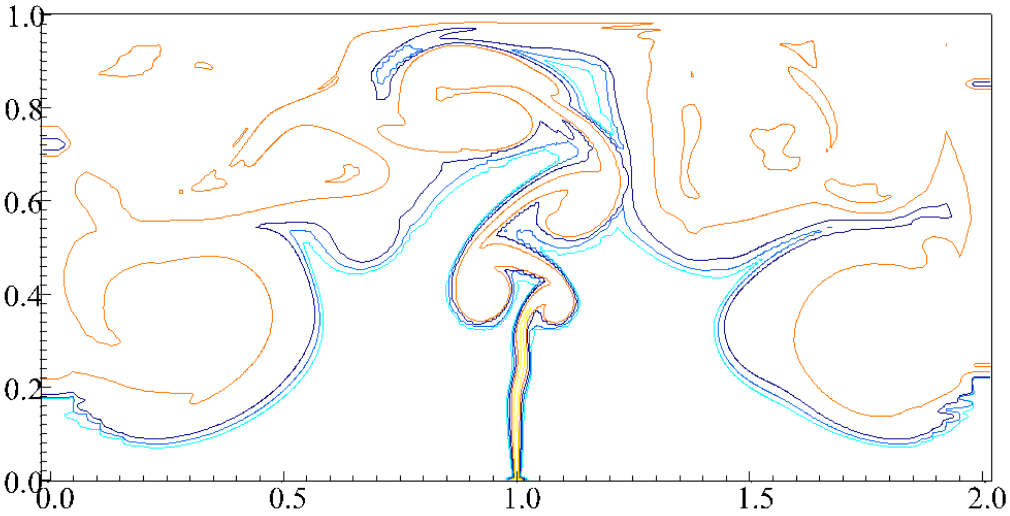

(a) t = 2568.75

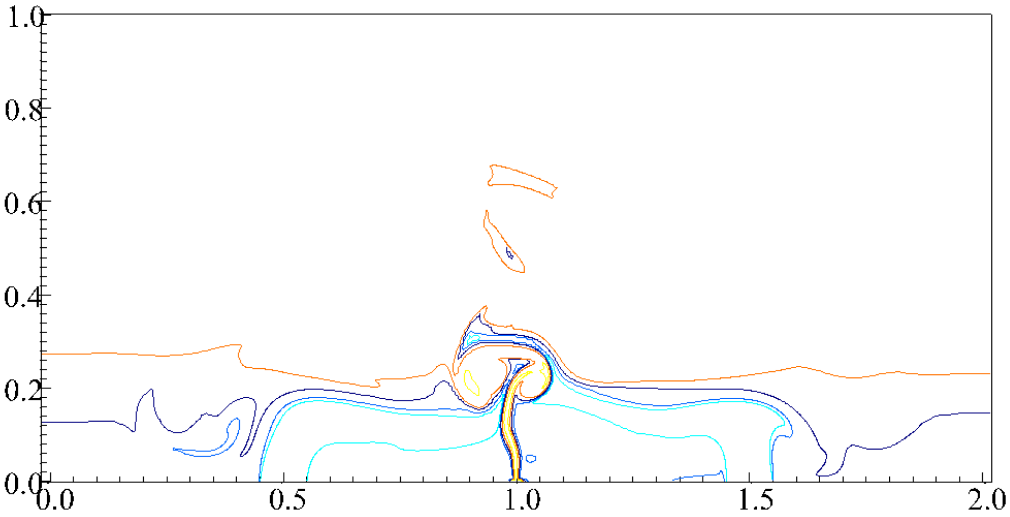

(b) t = ∞

Figure 8: Flow development over time for Pr = 7 and Re = 1.0×10^6. Figures 3a–4b and 6a–8b show temperature contours, whereas Figures 5a–5b show vorticity fields.

is accompanied by rebounding [14] and the formation of the new dipolar structures (Figures 4b and 5b). A similar behaviour was observed by Bastiaans et al. [4] and Orlandi [14]. The symmetric flow breaks down at $t \approx 800$ (Figure 4b), and sinuous instability occurs along the plume stem (Figure 6b) due to the horizontal shear [12]. This forms into a number of vortex structures along the plume stem at $t \approx 1200$ (Figure 7a). With time, the large scale recirculating flow develops and the fluid becomes stratified (Figures 7b and 8a). Finally, the flow reaches the fully developed state as shown in Figure 8b.

Figure 9 plots the vertical velocity component (v) at $y = 0.5$ along the plume axis over time for different Re and $Pr = 7$, showing the arrival and passage of the plume head, seen as the peak in the signal, the passage of the intrusion and finally breakdown into oscillatory flow. As shown in Figure 9, scaling relationships with Re are found empirically for initial peak velocity (v_{peak}), time taken to reach the initial peak velocity (t_{peak}) and time taken for the onset of instability (t_{turb}). These scalings provide a reasonable fit:

$$v_{peak} \sim Re^{-0.1587}, \tag{6}$$

$$t_{peak} \sim Re^{0.1728}, \tag{7}$$

$$t_{turb} \sim Re^{-0.4899}. \tag{8}$$

Equations (6)–(8) show that v_{peak} and t_{turb} decrease with increasing Re, while t_{peak} increases with Re. Observe that t_{turb} has a stronger dependence on Re than both v_{peak} and t_{peak}.

3.2 Flow turbulence

For the cases shown in Table 1, Figure 10 plots temporal spectra of the square of the vertical velocity fluctuation, v'^2, at $(x, y) = (1.0, 0.95)$ (that is, a location near the ceiling along the plume axis) against non-dimensional frequency, $St = f^*\tau$, where f^* is dimensional frequency and $\tau = H/U$ the characteristic time. As expected for two dimensional turbulence, the spectra follow the -3 power law in the inertial subrange [8, 9].

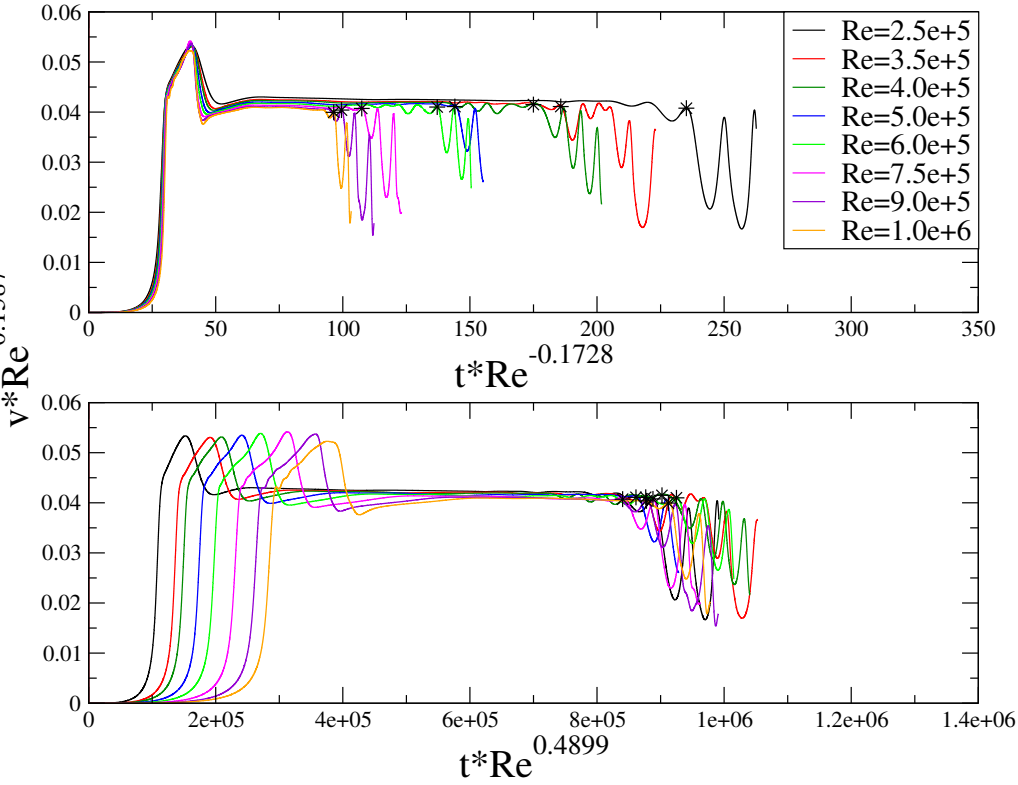

Figure 9: Variation of v at $y = 0.5$ along the plume axis over time for different Re and Pr = 7 (with t and v scaled with Re) plotted up to a point of the onset of turbulence, which is indicated by $*$.

Figure 10 shows the spectral amplitudes are smaller for higher Pr at constant Re (the same trend has been observed for spectra of v'^2 at $y = 0.15$ and 0.5). Also observe in the spectra that the transition from the approximately flat low frequency region to the inertial region shifts to the left with increasing Pr at constant Re, which suggests that in lower Pr flows, large amplitude motions occur at higher frequencies than for higher Pr. The $Pr = 0.7$ and 7 results show that for these cases the Re variation in the spectral amplitude is small. However, in the case of $Pr = 70$ a larger variation with Re is observed, with the spectral amplitudes larger for lower Re. For $Re = 5.0 \times 10^5$, the spectral amplitudes at low frequencies are about ten times larger than those at the higher Re.

To further examine the Re dependency of the $Pr = 70$ flow, instantaneous temperature fields are shown in Figures 11–12. Figures 11a and 11b show the flow behaviours at $Re = 5.0 \times 10^5$ at different times. In Figure 11a, the plume is seen to penetrate the upper, high temperature region, carrying unmixed fluid to the ceiling and forming vortical structures. Figure 11b shows unmixed heated plume fluid penetrating almost to the ceiling, with animations showing that at this time the plume is undergoing a large scale flapping motion adjacent to the ceiling. This large scale flapping could be associated with the large spectral amplitudes at low frequencies for this case (the results in Figure 10 have been obtained at $y = 0.95$). In the higher Re flow shown in Figure 12b, the plume undergoes mixing and dissipation at the interface, with very little penetration. However, for the lower Pr the variation in the heights at which the plume dissipates, over the given range of Re, was found to be much smaller.

3.3 Mean temperature field

Figure 13 plots the mean temperature against the domain height for each case shown in Table 1. The definition of mean temperature here is the same as in Figure 2. The interface between the lower ambient and upper buoyant

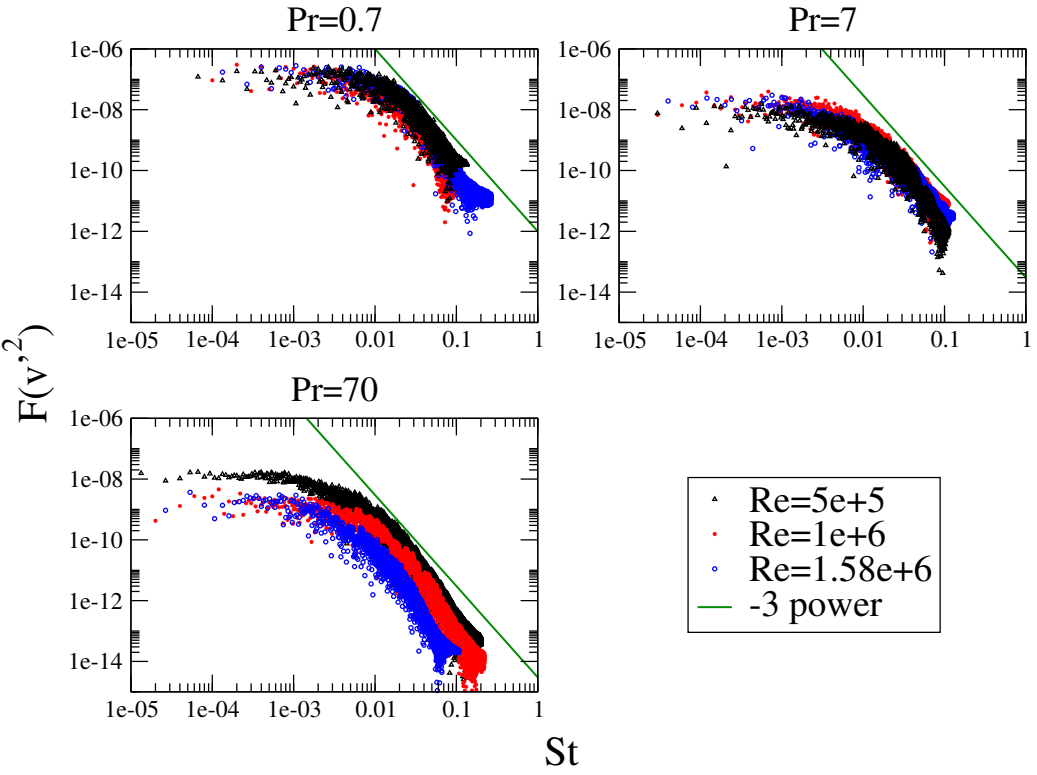

Figure 10: Temporal spectra of v'^2 at $y = 0.95$ along the plume axis for different Re and Pr.

layers is considered to be located in the region of the sudden increase in mean temperature [1]. It is seen that the interface is rather smeared out, which is different from the observation made by Linden et al. [11], but consistent with Kaye et al. [7].

It is observed that for the range of Re and Pr examined, the interface height is higher for higher Pr, at constant Re. For $Pr = 0.7$ and 7, the interface height varies only slightly with Re, for each case, while for $Pr = 70$ the $Re = 5.0 \times 10^5$ interface is significantly higher than for the other two Re, where it is similar.

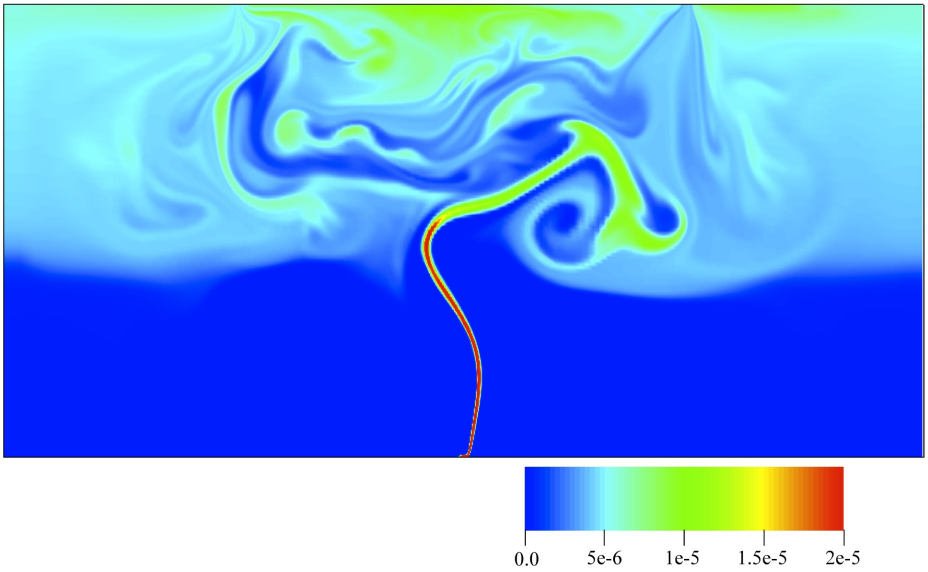

(a) $\mathrm{Re} = 5.0 \times 10^5$

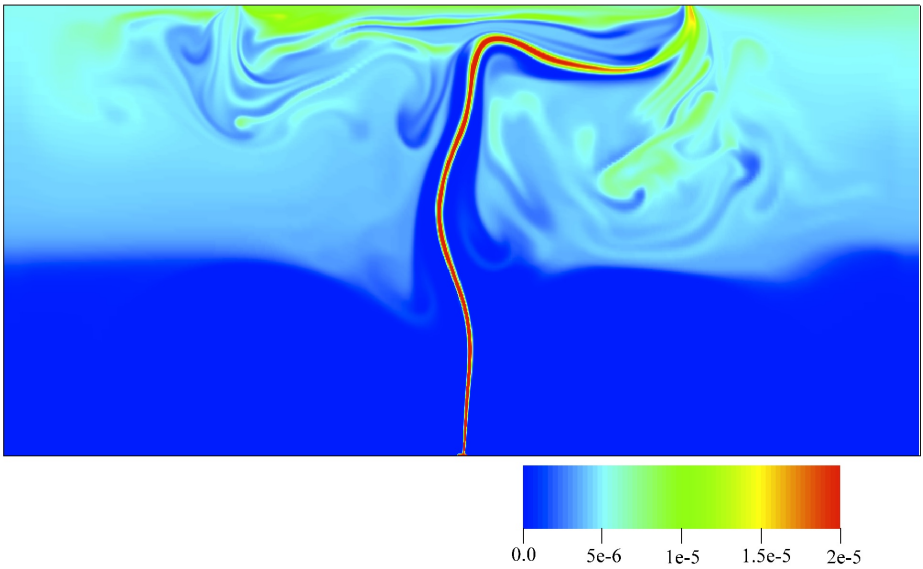

(b) $\mathrm{Re} = 5.0 \times 10^5$ (laminar flapping)

Figure 11: Temperature fields for $\mathrm{Pr} = 70$ and different Re.

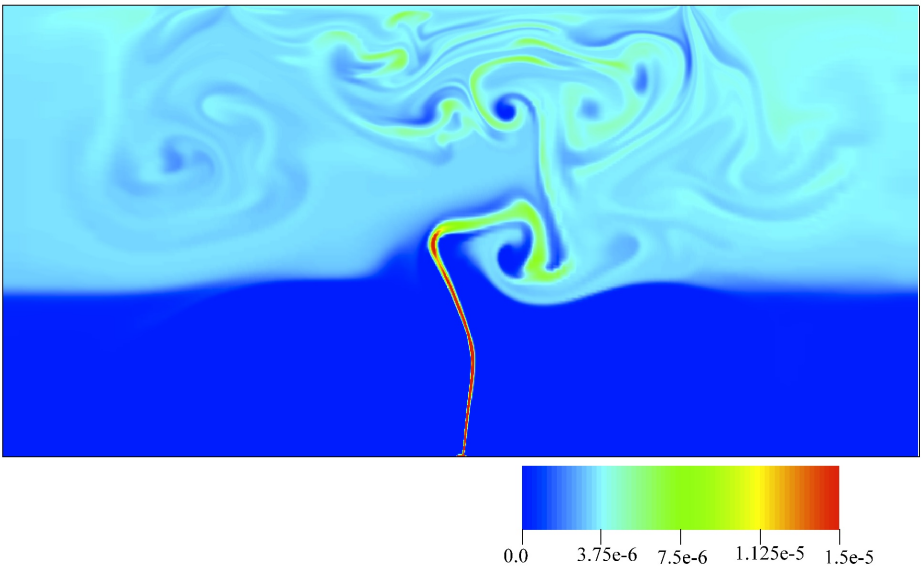

(a) $\mathrm{Re} = 1.0 \times 10^6$

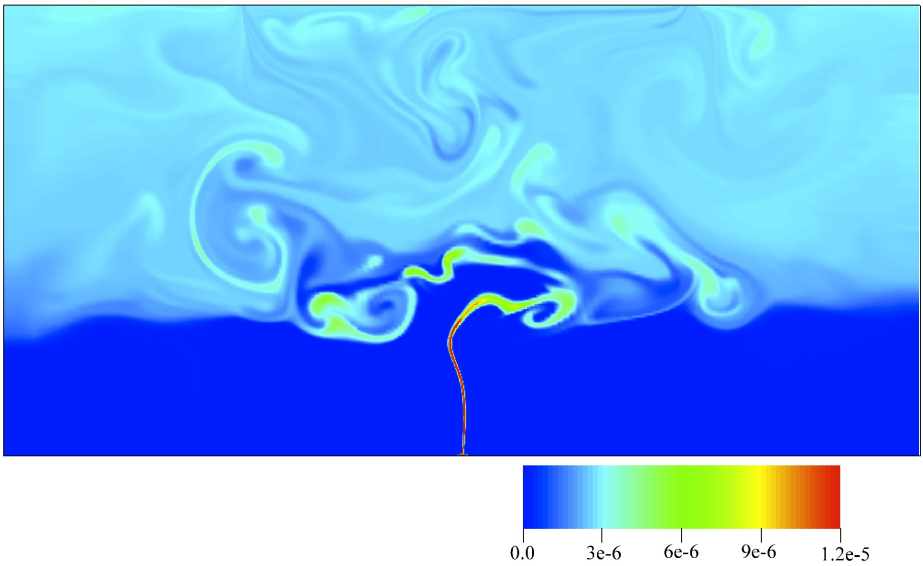

(b) $\mathrm{Re} = 1.58 \times 10^6$

Figure 12: Temperature fields for $\mathrm{Pr} = 70$ and different Re.

This may be due to the unmixed fluid of higher temperature near the ceiling, as indicated by the second sharp increase in mean temperature, at about $y = 0.9$ for $Re = 5.0 \times 10^5$, which is also shown in Figures 11a and 11b. Fluid of higher temperature has a higher buoyancy and increases the volume flow rate at the top openings [11], which may have led to a higher interface. The large scale, laminar flapping behaviour shown in Figure 11b suggests that diffusion by eddy formation is small in this case. Thus, a low level of mixing due to eddies generated by the rising plume seems to have led to the accumulation of the fluid with higher temperature near the ceiling.

The upper layer temperature is less uniform for higher Pr at a given Re, and for reduced Re, at $Pr = 7$ and 70. At $Pr = 0.7$ the upper layer temperature is approximately uniform for all Re. At $Pr = 7$ the uniformity reduces with reducing Re from $Re = 1.58 \times 10^6$, for which the upper layer temperature is approximately uniform. At $Pr = 70$ the upper layer temperature is not uniform for all Re, with the uniformity reducing with reducing Re. With increasing Re for $Pr = 7$ and 70, the increased mixing by eddies leads to a more uniform temperature distribution. The reduced uniformity at higher Pr at constant Re may be due to reduced thermal diffusivity, associated with increasing Pr, as well as reduced mixing by eddies, since spectral amplitudes are lower for higher Pr from Figure 10. Hence, a higher interface observed for higher Pr may be at least in part due to the accumulation of higher temperature fluid beneath the ceiling, with the resultant higher buoyancy increasing the flow rate.

4 Conclusion

The effects of Re and Pr on transitional natural ventilation flow were investigated using two dimensional simulations. The scaling relationships with Re are obtained for the start-up plume behaviour. The effects on flow turbulence and mean temperature field were also investigated for fully developed flow. It is found that spectral amplitudes reduce with increasing Pr. The interface

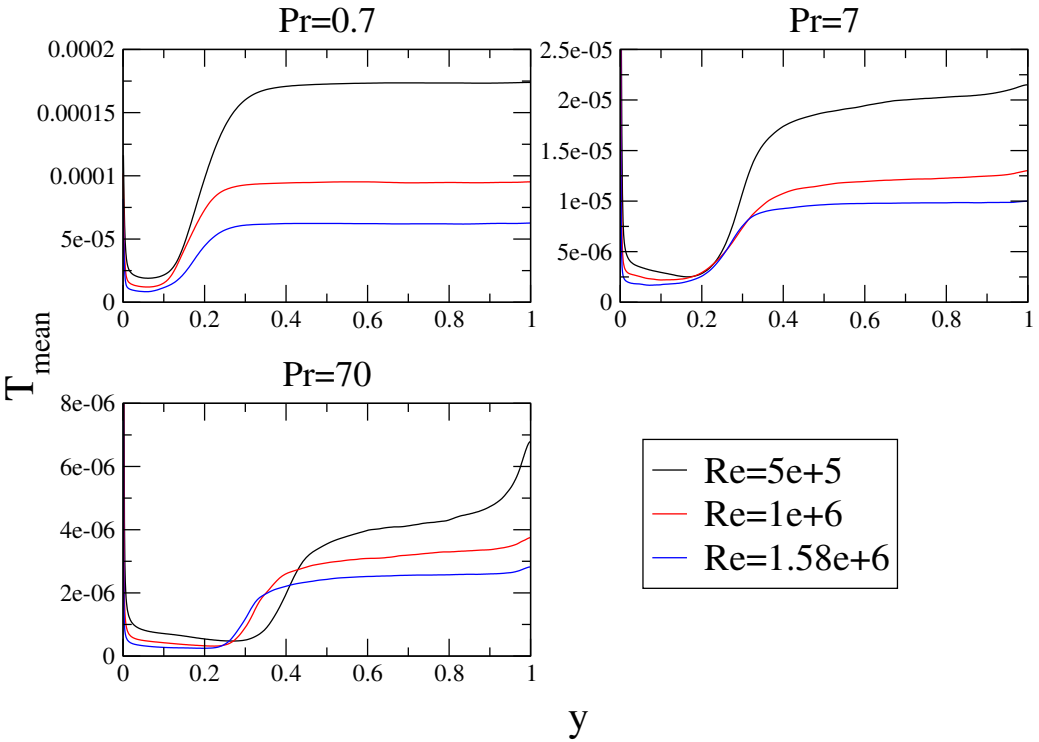

Figure 13: Mean temperature over height for different Re and Pr

is seen to be smeared out and its location varies with the parameter values. The upper layer temperature is shown to be more uniform at lower Pr, and for Pr = 7 and 70 it is more uniform at higher Re.

References

[1] I. E. Abdalla, M. J. Cook, S. J. Rees, and Z. Yang. Large–eddy simulation of buoyancy-driven natural ventilation in an enclosure with a

point heat source. *Int. J. Comput. Fluid Dyn.*, 21(5–6):231–45, 2007. doi:10.1080/10618560701599710 C1076

[2] S. W. Armfield. Ellipticity, accuracy, and convergence of the discrete Navier–Stokes equations. *J. Comput. Phys.*, 114(2):176–84, 1994. doi:10.1006/jcph.1994.1158 C1064

[3] S. W. Armfield and R. Street. An analysis and comparison of the time accuracy of fractional–step methods for the Navier–Stokes equations on staggered grids. *Int. J. Numer. Methods Fluids*, 38(3):255–82, January 2002. doi:10.1002/fld.217 C1064

[4] R. J. M. Bastiaans, C. C. M. Rindt, F. T. M. Nieuwstadt, and A. A. van Steenhoven. Direct and large-eddy simulation of the transition of two- and three-dimensional plane plumes in a confined enclosure. *Int. J. Heat Mass Transfer*, 43(13):2375–93, 2000. doi:10.1016/S0017-9310(99)00302-6 C1062, C1066, C1073

[5] G. K. Batchelor. Small-scale variation of convected quantities like temperature in turbulent fluid Part 1. general discussion and the case of small conductivity. *J.Fluid Mech.*, 5(01):113–33, 1959. doi:10.1017/S002211205900009X C1064

[6] Y. A. Gostintsev, L. A. Sukhanov, and A. F. Solodovnik. Steady self-similar turbulent plume above a point source of heat and matter. *Fluid Dynamics*, 18:273–8, 1983. doi:10.1007/BF01091118 C1061

[7] N. B. Kaye, Y. Ji, and M. J. Cook. Numerical simulation of transient flow development in a naturally ventilated room. *Building and Environment*, 44(5):889–897, May 2009. doi:10.1016/j.buildenv.2008.06.016 C1076

[8] R. H. Kraichnan. Inertial ranges in two-dimensional turbulence. *Phys. Fluids*, 10(7):1417–23, 1967. doi:10.1063/1.1762301 C1073

[9] R. H. Kraichnan and D. Montgomery. Two-dimensional turbulence. *Rep. Prog. Phys.*, 43(5):547–619, 1980. doi:10.1088/0034-4885/43/5/001 C1073

[10] B. P. Leonard and S. Mokhtari. Beyond first-order upwinding: The ultra-sharp alternative for non-oscillatory steady-state simulation of convection. *Int. J. Numer. Methods Eng.*, 30(4):729–66, 1990. doi:10.1002/nme.1620300412 C1063

[11] P. F. Linden, G. F. Laneserff, and D. A. Smeed. Emptying filling boxes—the fluid-mechanics of natural ventilation. *J. Fluid Mech.*, 212:309–35, 1990. doi:10.1017/S0022112090001987 C1061, C1062, C1076, C1079

[12] Yuen D. Majumder, C. and A. Vincent. Four dynamical regimes for a starting plume model. *Phys. Fluids*, 16(5):1516–31, 2004. doi:10.1063/1.1683151 C1073

[13] B. R. Morton, G. Taylor, and J. S. Turner. Turbulent gravitational convection from maintained and instantaneous sources. *Proc. R. Soc. London, Ser. A*, 234(1196):1–23, 1956. doi:10.1098/rspa.1956.0011 C1061

[14] P. Orlandi. Vortex dipole rebound from a wall. *Physics of Fluids A: Fluid Dynamics*, 2(8):1429–36, 1990. doi:10.1063/1.857591 C1073

Author addresses

1. **T. Hattori**, School of Aerospace, Mechanical and Mechatronic Engineering, The University of Sydney, Sydney, Australia. mailto:tae.hattori@sydney.edu.au

2. **S. W. Armfield**, School of Aerospace, Mechanical and Mechatronic Engineering, The University of Sydney, Sydney, Australia.

3. **M. P. Kirkpatrick**, School of Aerospace, Mechanical and Mechatronic Engineering, The University of Sydney, Sydney, Australia.